01 Jun 2019

Iterative Learning Control of Single Point Incremental Sheet Forming Process using Digital Image Correlation

Joseph D. Fischer

Mitchell R. Woodside

Mercedes M. Gonzalez

Nathan A. Lutes

et. al. For a complete list of authors, see https://scholarsmine.mst.edu/mec_aereng_facwork/4334

Recommended Citation

J. D. Fischer et al., "Iterative Learning Control of Single Point Incremental Sheet Forming Process using Digital Image Correlation," *Procedia Manufacturing*, vol. 34, pp. 940-949, Elsevier B.V., Jun 2019.
The definitive version is available at https://doi.org/10.1016/j.promfg.2019.06.108

Available online at www.sciencedirect.com

ScienceDirect

Procedia Manufacturing 34 (2019) 940–949

Procedia MANUFACTURING

www.elsevier.com/locate/procedia

47th SME North American Manufacturing Research Conference, Penn State Behrend Erie, Pennsylvania, 2019

Iterative learning control of single point incremental sheet forming process using digital image correlation

Joseph D. Fischer, Mitchell R. Woodside, Mercedes M. Gonzalez, Nathan A. Lutes, Douglas A. Bristow*, Robert G. Landers

Missouri University of Science and Technology, 194 Toomey Hall, MO, 65409, USA

*Corresponding author. Tel.: +1-573-341-6559; *E-mail address:* dbristow@mst.edu

Abstract

Single Point Incremental Sheet Forming (SPIF) is a versatile forming process that has gained significant traction over the past few decades. Its increased formability, quick part adaption, and reduced set-up costs make it an economical choice for small batch and rapid prototype forming applications when compared to traditional stamping processes. However, a common problem with the SPIF process is its tendency to produce high geometric error due to the lack of supporting dies and molds. While geometric error has been a primary focus of recent research, it is still significantly larger for SPIF than traditional forming processes. In this paper, the convergence behavior and the ability to reduce geometric error using a simple Iterative Learning Control (ILC) algorithm is studied with two different forming methods. For both methods a tool path for the desired reference geometry is generated and a part is formed. A Digital Image Correlation (DIC) system takes a measurement and the geometric error along the tool path is calculated. The ILC algorithm then uses the geometric error to alter the tool path for the next forming iteration. The first method, the Single Sheet Forming (SSF) method, performs each iteration on the same sheet. The second method, the Multi Sheet Forming (MSF) method, performs each iteration on a newly replaced sheet. Multiple experiments proved the capability of each method at reducing geometric error. It was concluded that using the MSF method allows for negative corrections to the forming part and, therefore, leads to better final part accuracy. However, this method is less cost effective and more time consuming than using the standard SSF methodology. In addition, it was found that in order to effectively correct a part with an ILC algorithm, steps must be taken to increase the controllability of the part geometry.

Keywords: Incremental Sheet Forming; Iterative Learning Control; Feedback Control; Digital Image Correlation

1. Introduction

Asymmetrical Incremental Sheet forming, commonly referred to as Incremental Sheet Forming (ISF), is a unique method of forming sheet metal when compared to traditional forming processes such as spinning and deep drawing. Advancements in CNC machinery and CAM path planning software have increased the feasibility of this process over the past few decades [1]-[4]. Its superior formability, quick implementation, and reduced set-up costs [5] make it ideal for small batch production and rapid prototyping of sheet metal parts [3] in contrast with traditional stamping processes which require the fabrication of expensive dies for each unique geometry.

In Single Point Incremental Sheet Forming (SPIF), a sub-class of ISF, a single point of contact is used to form a constrained sheet metal blank. This is typically done by locally deforming the sheet metal with a forming tool on one side while the other side of the sheet is completely un-supported. This process is truly die-less, and, in theory, the most flexible of the ISF sub-classes. However, this lack of

10.1016/j.promfg.2019.06.108

support tends to be the primary cause of geometric errors [3].

As a result, substantial research has been conducted over the past decade to address the issues of geometric inaccuracy in SPIF [5]. Of which, only a few have focused on feedback control as the primary solution [4]. Some of the most recent work involving geometric error feedback control include the implementation of an ILC algorithm that corrects CAD geometry [6, 7] and the use of adaptive regression splines to predict error of a part based on its features [8].

This paper examines Single Sheet Forming and Multi-Sheet Forming methods for closed loop feedback control. Both methods incorporate the use of a parallel kinematic industrial robot, a DIC system, and an ILC control algorithm to reduce the geometric inaccuracies in a standard SPIF process. Of the three elements in this process, only a handful of other publications have employed digital image correlation into the correction of ISF processes. [9, 10]. The goal of the research conducted in this paper is to examine the convergence behavior of the ILC algorithm developed for the SPIF process using various forming methodologies. Specifically, this paper focuses on two different forming methods: the Single Sheet Forming (SSF) and the Multi-Sheet Forming (MSF) methods. It is found that by replacing the sheet after each iteration, which allows for negative correction, the error never increased with subsequent iterations. This is not the case when using the SSF method.

In the first section, this paper will discuss the structure of the ILC correction algorithm, in addition to a brief summary of the SSF and MSF methodologies. After this discussion, the next section will describe the SPIF equipment setup including the robotic forming machine, forming tool, and the measurement system. In the final section, the results of multiple forming experiments of the SSF and MSF methodologies are compared for their effectiveness in reducing geometric error of a formed part.

Nomenclature

x	x-coordinate of tool path (mm)
y	y-coordinate of tool path (mm)
z	z-coordinate of tool path (mm)
k	correction coefficient
e	error (mm)
j	iteration number
p	point index
z_{ref}	z-coordinate of reference (mm)
z_m	z-coordinate of measurement (mm)
MSF	multi-sheet forming
SSF	single sheet forming

2. Method

2.1. ILC Algorithm

The ILC algorithm used in this paper is an adaption of the common iteration-based algorithm originally proposed by Arimoto et al. [11]. In ILC, the future response of a repetitive process is corrected by a system's previous response over multiple iterations. Similarly, in this work's process, a tool path of three-dimensional points is corrected over multiple iterations of a repetitive forming process.

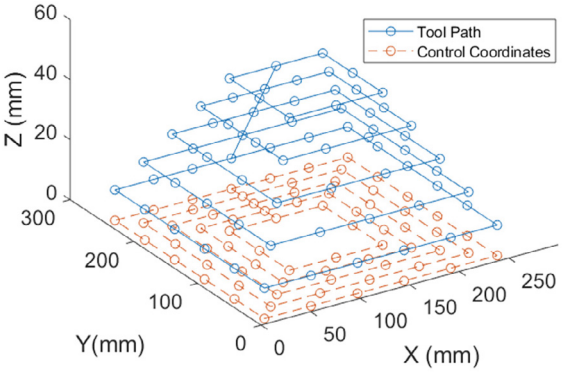

Fig. 1. Tool path and corresponding control coordinates

Due to the complexity of spatial correction and DIC data acquisition practices, the algorithm in this paper is based on the concept of controlling the magnitude of the displacement in the forming, or *z* direction. This method creates a set of new *z* coordinates for every point in the iteration's tool path. In addition to a *z* coordinate, each point in the toolpath has a unique *x* and *y* coordinate which are both held constant throughout every iteration of the process. These constant *x* and *y* coordinates form a set called the control coordinates. The union of *z* coordinates and control coordinates create the three-dimensional tool path for the robot to follow. An illustration of a simplified tool path and its corresponding control coordinates are shown in Figure 1. The toolpath used in this paper has 15,625 points while the number of points in the illustration is significantly reduced for clarity. The coordinates for the next iteration's tool path are then given by,

$$x(j+1,p) = x(j,p), \tag{1}$$

$$y(j+1,p) = y(j,p), \tag{2}$$

$$z(j+1,p) = z(j,p) + ke(j,p), \tag{3}$$

where *x* and *y* are the control coordinates, *z* is the corrected coordinate in the *z*-direction, *k* is the correction factor, *e* is the *z*-direction error, *j* is the current iteration number, and *p* is the index of the point in each iteration's tool path.

In practice, the correction factor, *k* is bounded by 0 and 1 to prevent over-forming. On each iteration, a portion of the error magnitude corresponding to the correction factor is added in the *z*-direction to the tool path at each control coordinate. This factor was selected at the beginning of the experiment and remained constant throughout subsequent iterations. The *z* displacement error is defined as

$$e(j,p) = z_{ref}(p) - z_m(j,p) \tag{4}$$

where z_{ref} is the z coordinate of the reference, or desired shape, at each control coordinate and z_m is the z coordinate of the measured geometry at the same control coordinate. Figure 2 shows an example of the error for a single measured point on a part surface.

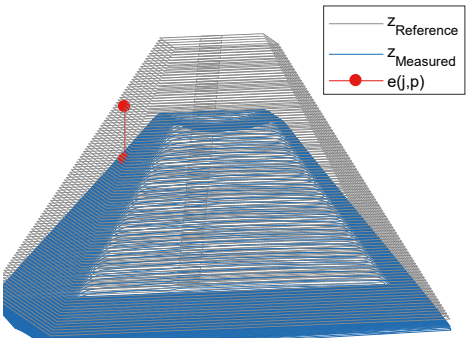

Fig 2. Error between reference and measured part surface

2.2. Single and Multi-Sheet Forming Methods

In the SSF method a reference part geometry with corresponding control coordinates is selected, a sheet is secured to the frame, and an initial measurement is made by the DIC system. Using the reference geometry, control coordinates, and DIC measurements, the correction algorithm detailed in the previous section generates a toolpath. This toolpath is executed by the robot, completing the first iteration of the SSF method. This portion of the method is shown by the black path in Figure 3.

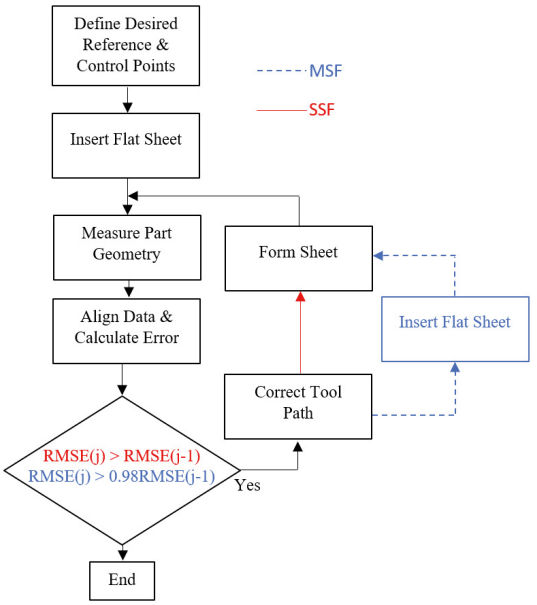

Fig. 3. SSF and MSF method diagram

On subsequent iterations the part is measured, the tool path is updated using the correction algorithm, and the same sheet is reformed. This method is repeated until the stopping criteria, detailed in section 4.3, is met. The SSF method is shown by the red path in Figure 3.

The MSF method is similar in structure to the SSF Method. The primary difference between the two methods is that the formed sheet is measured, removed, and replaced with a new sheet after each iteration in the MSF method. This procedure is repeated for every iteration in the MSF method until the stopping criteria is met. The MSF method is shown by the blue path in Figure 3.

3. Experimental Setup

3.1. Robot and Forming Tool

The forming machine used in this research is an ABB IRB 940 Tricept parallel kinematic robot (Figure 4). Analysis of a robot with a similar kinematic structure was performed by Callegari et al. [12] for its use in ISF processes.

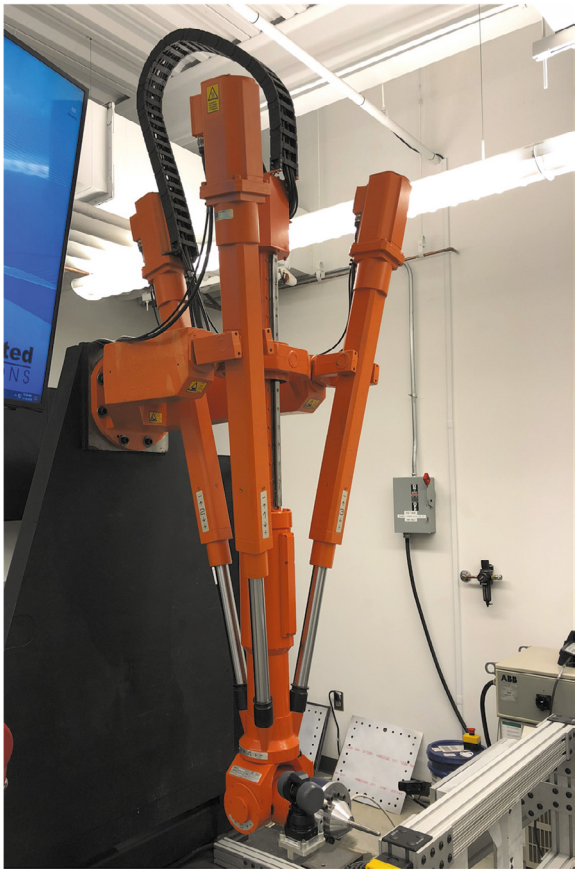

Fig. 4. ABB IRB 940 Robot

A calibration of all six axes of the IRB 940 was performed according to the manufacturer's specifications. The image in Figure 5 depicts the robot and the sheet metal blank clamping frame. In order to simplify the coordinates used for forming tool paths, a coordinate system was digitally attached to the frame and used as the primary coordinate system for robot operation. This coordinate frame

and coordinate system will be referred to as the work object frame and work object coordinate system, respectively. These coordinate frames are also depicted in Figure 5.

In order to define the work object coordinate frame, measurements of the base structure and the clamping frame were performed using an Automated Precision, Inc. model R-20 Radian laser tracker in combination with New River Kinematics' Spatial Analyzer (SA) software. According to the manufacturer specifications, the laser tracker measurement's standard deviation is 2.5 μm and was deemed sufficient in determining the rigid transformation between the robot's base frame and the work object frame. The work object frame was measured by using a Surface Mounted Reflector (SMR) measurement probe.

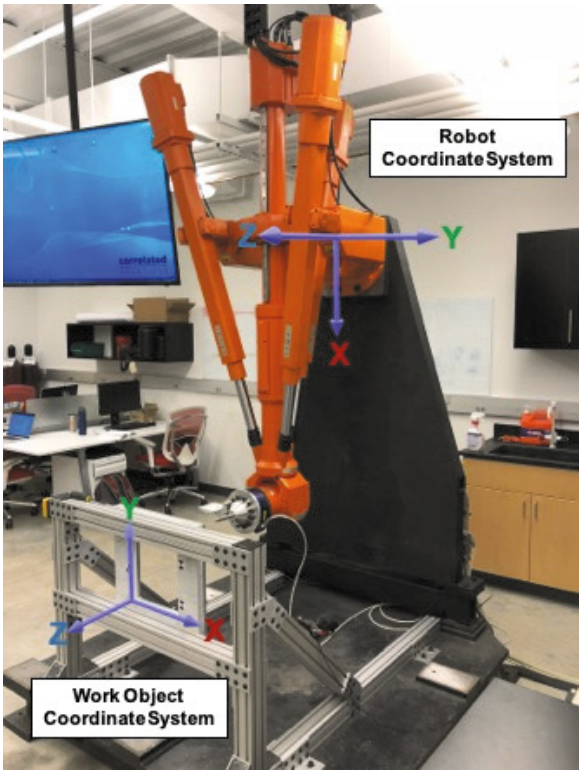

Fig. 5. Robot and clamping frame with coordinate systems

The forming tool, shown in Figure 6, is comprised of a spherical tool tip made out of M2 high speed steel (M2 HSS) that has been press fit into a conical aluminum hub. The tool tip and hub sub-assembly are bolted to a circular aluminum plate. The forming tool assembly is attached to a JR3 six axis force sensor that is bolted to the robot's end effector. In future research the force sensor will be used in accordance with a TTL trigger to acquire live force data during the forming process.

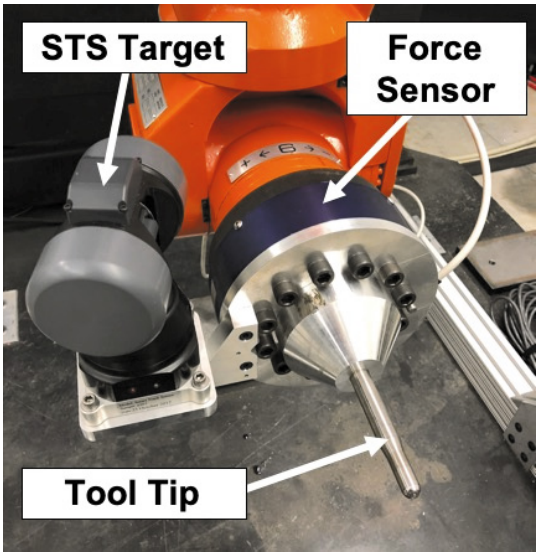

Fig. 6. Forming Tool Assembly

In Figure 6, an aluminum platform is mounted to the left side of the forming tool assembly. This platform is designed to facilitate an API Smart Track active laser target that is used in conjunction with the Radian laser tracker and SA software. Together, this equipment is used to measure the static transformation between the robot's initial tool frame and the tool frame of the forming tool assembly.

3.2. Digital Image Correlation

A Correlated Solution's DIC system (Figure 7) was used to measure the displacement of the formed parts in the SPIF process. This physical system is composed of two cameras mounted to a single tripod. The DIC requires ample light on the measurement specimen. For this process three led lights were used to completely illuminate the sheet metal blank.

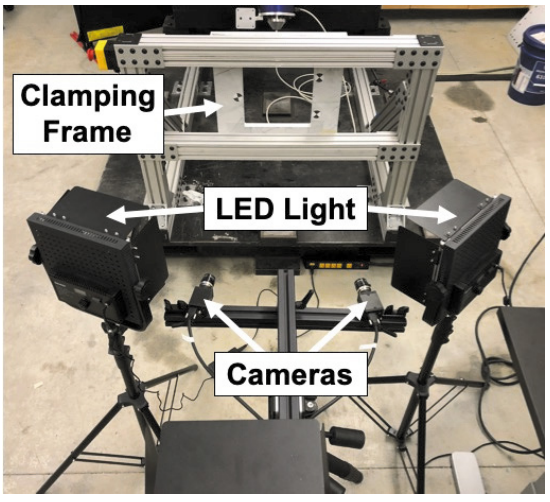

Fig. 7. DIC system

The system's cameras monitor a unique speckle pattern applied to the part's surface at the beginning of the process. As the specimen is deformed, the speckle pattern displaces. The displacement of the speckle pattern in subsequent images is compared by a grouping of neighboring pixels called a subset. Each speckle pattern is composed of many subsets, and a maximization function is used to locate each subset in relation to the reference image [10]. The displacements of each of the subsets are calculated and used to determine the 3D displacement of the deformed surface. The main advantage of this system is that other measurements, such as strain and wall thickness, can be calculated based on the relative movement between the individual subsets. In future work, these additional measurements will be utilized.

The DIC system is calibrated at the beginning of each forming experiment. Each camera is centered at approximately the same point on the clamping frame and each lens is focused on the measurement specimen. An aluminum calibration block, with a known grid size, is oriented in front of the cameras and several pictures are taken of the calibration block at different orientations. There are several calibration blocks with different grid sizes to choose from. The 14 mm calibration block was selected for this process.

Images collected during the calibration process are run through a calibration algorithm in VIC-3D, which is a DIC analysis software developed by Correlated Solutions. From this algorithm, a single coordinate frame, known as the camera coordinate frame, is defined relative to both cameras. This coordinate frame will be called the camera coordinate frame. The deformation of the measurement specimen is described relative to this coordinate frame.

Once the calibration images have been collected and validated, an initial reference image is taken, and the forming experiment is executed. For this process, only an initial reference image and an image of the final deformed part are needed; however, another program called VIC-Snap can be used to take images at different time intervals. This could be used in future work to analyze the strain induced in the sheet metal part during the entire process.

After all process images have been collected, they are imported into VIC-3D and analyzed using the method discussed previously. Once all selected images have been analyzed, their data is stored in a VIC-3D file format that can be accessed through both VIC-3D or a VIC-3D specific python library. The latter is used for this process.

3.3. Coordinate System Alignment – Robot and DIC

All of the data analyzed in the VIC-3D software was measured relative to the camera's coordinate frame. In order to calculate an error correction that can be directly applied to the robot's tool path, the data measured by VIC 3D must be transformed into the work object coordinate system.

The camera coordinate frame changes location and orientation for every camera re-calibration. VIC-3D has a built-in feature that is capable of detecting the center of target markers and using their location, relative to the work object coordinate frame, to determine a transformation between the camera and work object coordinate frames. This transformation creates a coarse alignment between the two coordinate systems. In order to more accurately align the data, an error minimization technique was used in addition to the previous calibration method. Both methods effectively and accurately transformed the data into the work object coordinate system from the camera's coordinate system.

3.4. LabVIEW Control and Data Alignment

The forming, measurement, and correction sub-process require the use of multiple software platforms. Of these platforms, the main two being used are MATLAB and VIC-3D. A Virtual Instrument (VI) was developed in LabVIEW to combine the data acquisition and analysis functionality of VIC-3D with the data manipulation functionality of MATLAB to create a completely automated process.

4. Results

4.1. General Experimental Parameters

Several process parameters remained fixed during all the experiments conducted in this paper. The tooltip diameter was 12.7 mm and moved at a speed of 42.5 mm/s. The height and width of the work area were both 254 mm. The forming material used was 1.6 mm thick 6061-O aluminum.

Due to its simple geometry and the ability to compare it with previous works [13], a truncated pyramid was selected as the test part. The general dimensions for the truncated pyramid used in this paper are shown in Table 1 and Figure 8.

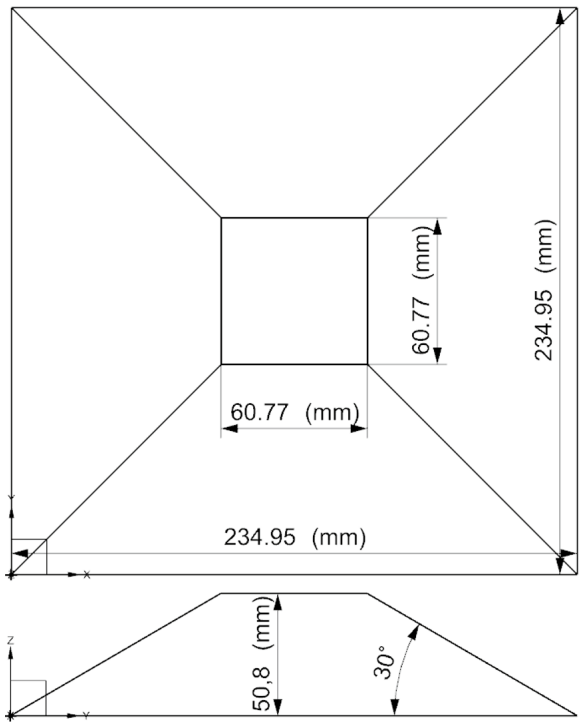

Fig. 8. Pyramid dimensions.

Table 1. Truncated pyramid dimensions.

Parameter	Dimension
Total Depth	50.80 mm
Base Width	234.95 mm
Base Height	234.95 mm
Wall Angle	30°
Truncated Region Width	60.77 mm

The control coordinates – and thus the tool paths – for this shape were positioned in order to correct the region along the oblique walls only and did not contain the truncated region (top) of the pyramid. As such, the error analyzed in this paper was only along the oblique walls and was calculated at each control coordinate. The projection of the two-dimensional control coordinates onto a measured part is shown in Figure 9.

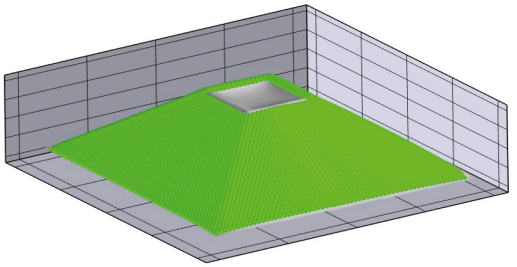

Fig. 9. Control coordinates projected onto formed part.

4.2. SSF Method Results

Three different correction factors were tested using the SSF methodology described in Section 2.2. These correction factors were selected in order to observe the performance capabilities of the closed loop system. These factors were chosen to be 0.25, 0.50, and 0.75 in order to sufficiently span the optimal range of the correction factor. Given material and time limitations, only three correction factors were examined in this study. The range was determined to be from 0 to 1, since gains that are larger than this would tend to over form the sheet. The stop criteria for this method was an increase in error from one iteration to the next. The results of the RMSE with respect to the reference geometry for the SSF method are shown in Table 2.

Table 2. SSF performance for different correction factors.

Correction Factor	**Minimum RMSE (mm)**	**Iterations to Minimum RMSE**
0.25	1.13	14
0.50	1.43	5
0.75	1.52	3

An important observation is that increasing the correction factor reduces the number of iterations necessary to reach a minimum error. However, it also results in lower geometric accuracy. This trend is a direct result of the tendency for higher correction factors to over form the part (i.e., form past the reference geometry). As higher correction factors are used, the part begins to over form in fewer iterations. When the number of iterations until significant over forming occurs is sufficiently low, the number of corrections executed by the control algorithm is also small. A low number of corrections reduces its ability to correct the part effectively, since the controller has fewer opportunities to implement an improved tool path. This essentially reduces the resolution of the control algorithm and its ability to apply fine corrections.

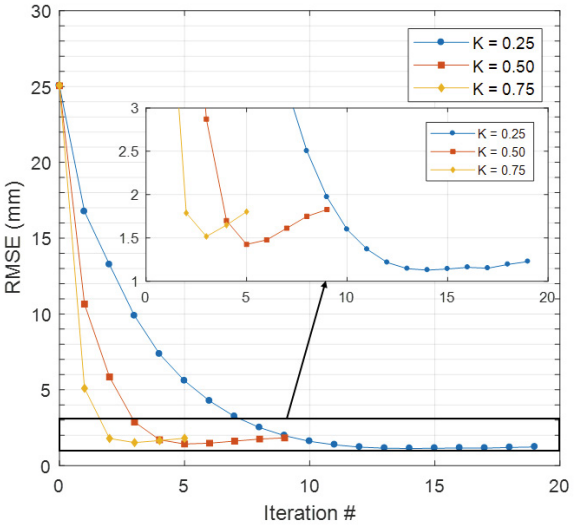

Fig. 10. Error progression for different correction factors using the SSF method.

Figure 10 shows the RMSE progression for each correction factor of the SSF method. An important observation is that the RMS error does not converge to a minimum value for any of the correction factors. Instead, the error reaches a minimum value after several iterations and then begins to increase. This increase in error is illustrated in Figure 11, which displays the cross section of the truncated pyramid for the final iteration, the iteration with minimum error, and the reference geometry.

An intriguing result is that the error near the top of the pyramid, approximately 30-40 mm from the center, is improved at the final iteration. However, the region near the middle and base of the oblique walls, approximately 45-115 mm from the center, suffers a significant increase in error, even though much of that region was not contacted by the tool after the RMS error reached a minimum value. This phenomenon is a result of non-localized deformations caused by the material being bent outward due to the force applied at the tooltip. Consequently, forming in one region of the part often negatively affects other regions by causing them to over form. Once a region has been over formed, it cannot be corrected with traditional, single direction SPIF techniques.

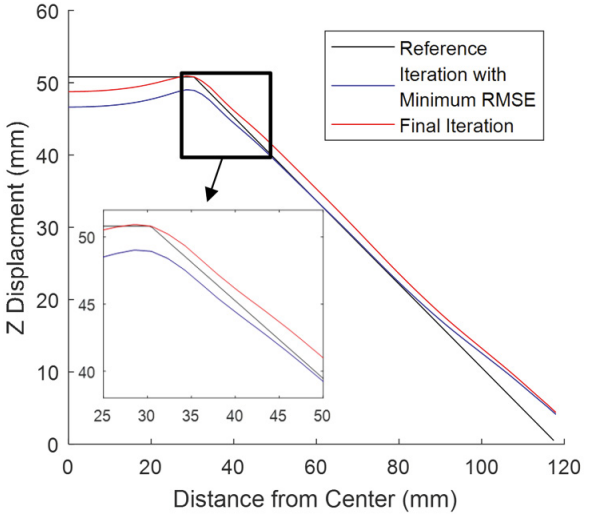

Fig. 11. Cross section of the measured data from final and minimum error iterations.

4.3. MSF Method Results

The inability to apply negative corrections is a drawback inherent to the SSF method. A means to address this shortcoming is to use the MSF method detailed in Section 2.2. This method was tested with the same process parameters detailed in Section 4.1. The stop criteria for the MSF method was when a 2% or less error reduction occurred from one iteration to the next.

Table 3 shows the results of using the SSF and MSF methods for the same correction factor of 0.5. An interesting observation is that the RMS error for the MSF method was reduced from 1.43 to 1.10 mm. This decrease in error is significant and corresponds to a reduction of approximately 23% when compared to the SSF method.

Table 3. Performance for SSF and MSF method with $k = 0.5$.

Forming Method	Minimum RMSE (mm)	Iterations to Minimum RMSE
SSF	1.43	5
MSF	1.10	8

Figure 12 shows the displacement progression for the final four iterations of the MSF method experiment. In contrast to the SSF displacement progression in Figure 11, the MSF method achieved extremely tight geometric control between iterations along the middle and base of the oblique walls. In addition, this method exhibits the ability to effectively correct under formed regions without significantly reducing the accuracy in other regions of the pyramid. This is shown in the top corner of the contour in Figure 12. As the iterations progressed, the error in this region was reduced, without substantial over forming in other regions such as the middle and base of the oblique wall. As such, this method not only reduced the final geometric error of the part, but it also kept the error from increasing away from the minimum value.

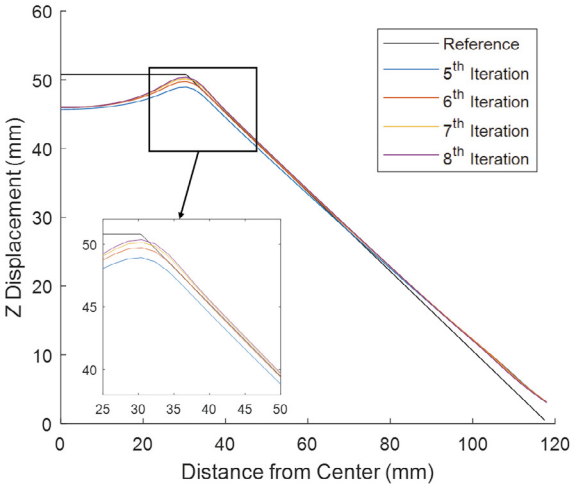

Fig. 12. Displacement progression for final four iterations of the MSF method ($k = 0.5$).

Another significant observation can be made by comparing the number of iterations taken to reach the lowest RMSE between the different methods. While the SSF method reaches a minimum RMSE value on its 5th iteration, the lowest RMSE value obtained from the MSF method was on the its 8th and final iteration. In contrast to the SSF method, the RMS error did not increase over a similar number of iterations. This suggests that replacing the sheet after each iteration reduces the tendency for the RMSE to diverge. This trend is shown clearly in RMSE progression of both methods in Figure 13. This effect is a result of the more precise control when using the MSF method.

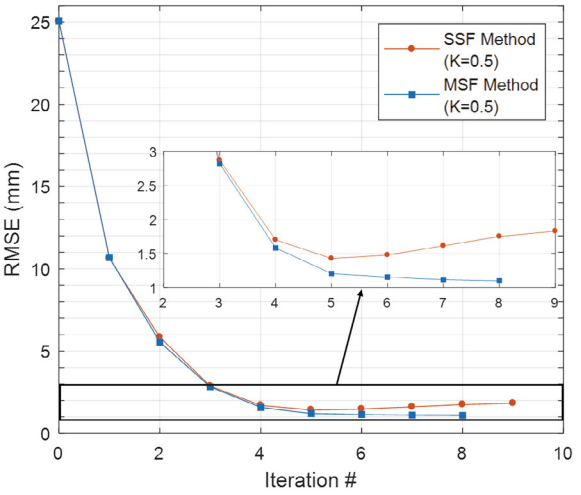

Fig. 13. Error progression for SSF and MSF methods.

The main factor that contributes to the tighter and more accurate control of the MSF method is its ability to provide negative feedback to the system. This is a result of replacing the sheet before each new tool path is executed. As such, a negative correction of the tool path results in less forming in the area that had been over formed on the previous iteration. This allows for more precise control of the system, especially

on the final iterations when the sheet is more likely to have been over formed.

4.4. System Controllability

An important observation can be made by examining Figures 11 and 12. Near the base of the oblique walls, approximately 80-120 mm from the center of the pyramid, the part is over formed significantly, regardless of the method used. This over forming near the base, which is caused by the sheet bending effect [5], contributes significantly to the geometric error of the part.

This type of error is caused by attempting to form a sharp angle in an unsupported region of the sheet. This is illustrated in the orange circle of Figure 14. These types of sharp angles, if left unsupported, are impossible to form without significant error when using the SPIF methodology [5]. The inability to control this region, is commonly referred to as the uncontrollability of the system [14]. By removing the data that lie in this uncontrollable region and recalculating the RMSE, the control scheme can be more accurately validated.

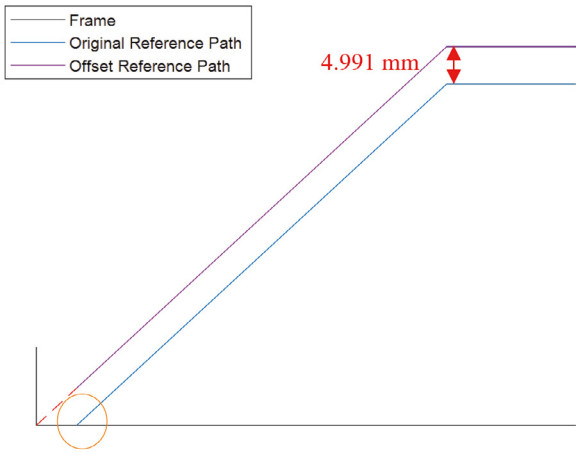

Fig. 14. Offset reference illustration.

The uncontrollable region was defined as any control coordinate with an x or y coordinate that was greater than 80 mm from the center. This area was chosen since the error from the bending effect was unsubstantial in this region. This square region is shown in Figure 15.

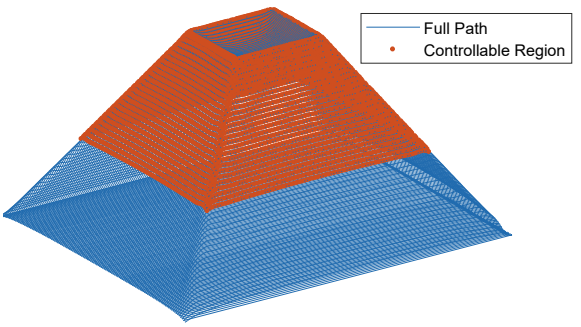

Fig. 15. Controllable (orange) and uncontrollable (blue) regions.

The RMS error for the controllable region was recalculated for the MSF and SSF experiments with $k = 0.5$. The results of this error calculation are shown in Table 4. The controllable region of the SSF method had a percent reduction of the RMSE value of 67.6% when compared to the results in Table 3, which included the uncontrollable region. The controllable region of the MSF method had a similarly reduced value of 72.8%.

Table 4. Performance for SSF and MSF method with $k = 0.5$ for controllable region.

Forming Method	Minimum RMSE (mm)	Iterations to Minimum RMSE
SSF (Contr. Region)	0.464	6
MSF (Contr. Region)	0.299	7

A scheme was developed to expand the controllable region to cover the entirety of all four oblique walls. This was accomplished by offsetting the reference part geometry such that if the oblique walls were extended, they would intersect the inside edges of the clamping frame, utilizing the full support of the clamping frame in the forming process. This offset is shown by the purple contour in Figure 14.

Two different experiments were performed using the offset reference. Each experiment used $k = 0.5$, with the process parameters in Section 5.1 held constant. The results of these experiments are shown in the Table 5.

Table 5. Performance for SSF and MSF method with correction factor 0.5 for offset reference

Forming Method	Minimum RMSE (mm)	Iterations to Minimum RMSE
SSF (Offset)	0.590	6
MSF (Offset)	0.300	8

The percent reduction of RMSE for the offset reference SSF and MSF methods were 58.7% and 72.7%, respectively. In comparison, the percent reduction of RMSE in the controllable region of the non-offset SSF and MSF methods were 67.6% and 72.8%, respectively. Although there is some discrepancy for the SSF method, the similarity between the percent reduction of RSME of the offset and the controllable region of the non-offset methods strongly indicates that the controllability of the forming process has been increased by offsetting the reference.

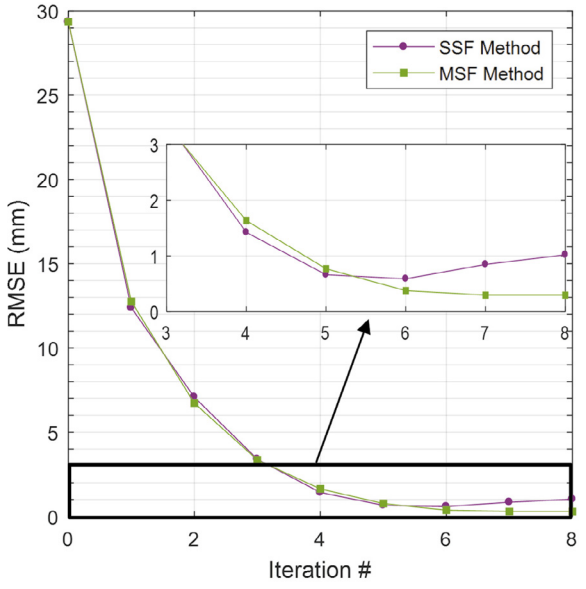

Fig. 16. Error progression for SSF and MSF methods using offset reference.

The RMSE progression for both the SSF and MSF methods when using an offset reference is shown Figure 16. As mentioned in Section 5.3, the results again show that the RMSE of the MSF method is not only lower overall than the SSF method, but it also resists increasing regardless of whether an offset reference is used.

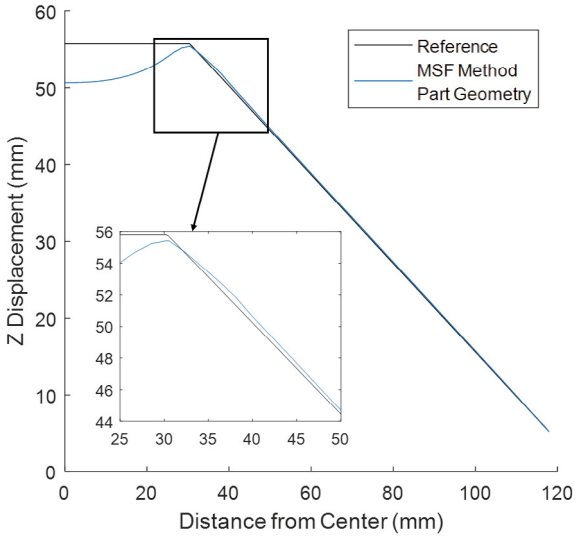

Fig.17. Final displacement of MSF method with offset reference.

The offset reference MSF method had the lowest RMSE when compared to the other experimental methods. These results are shown graphically in Figures 17 and 18, which show the displacement and the error surface of the part after the final iteration, respectively. These show that along the form path the geometric error is significantly reduced.

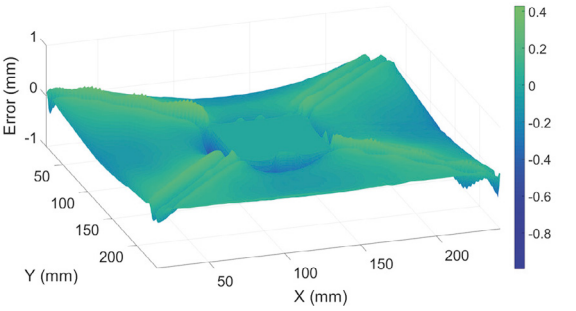

Fig. 18. Error surface over tool path for MSF method with offset reference (final iteration).

Figures 19 display the frequency distribution of the error for the MSF method with non-offset and offset reference techniques, respectively. It is observed that the offset reference frequency plot has a more evenly distributed geometric error when compared to the non-offset reference frequency plot. From this and previous observations, it can be concluded that the MSF method that utilizes the offset reference technique produces the lowest and more evenly distributed geometric error than any other previously tested method.

The negative errors in Figures 19 indicate regions that have been over formed. The tendency for the non-offset geometry to have a higher percentage of points which have negative error indicate that there is more over forming with this part. This is confirmed by looking at Figures 12 and 17 which show the final iteration's displacement of these two experiments. Along the middle and base of the pyramid, the non-offset reference experiences significant over forming due to factors mentioned above. However, by offsetting the reference and thereby increasing the controllability, these errors are significantly reduced.

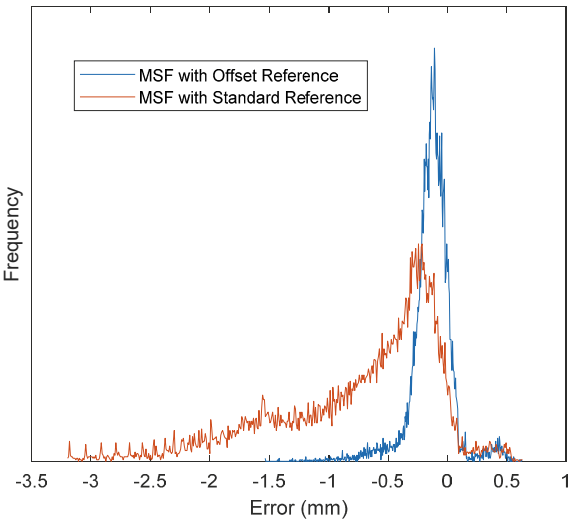

Fig. 19. Frequency distribution of error for MSF offset method.

5. Summary and Conclusions

The ILC algorithm with DIC measurement described in this paper was determined to be a suitable method in which

to correct geometric error of a formed part. The most accurate form had a total RMS error of 0.3 mm in accordance with an error frequency of ± 0.5 mm. In addition, the error was shown to resist diverging when using the MSF method. This validates not only the control algorithm, but also DIC as the primary measurement system for closed loop feedback control.

When forming with the SSF method, once a part becomes over formed, it cannot be corrected. Any negative corrections applied to the form path result in a failure for the tooltip to contact the sheet in that region. However, with the MSF method, a negative correction causes less forming in that region since the sheet is replaced before every form path. The ability to apply negative corrections allows for more precise control of the system and reduces the tendency for the error to diverge from the minimum. The result is that greater geometric accuracy can be achieved with this method than with the SSF method. However, a drawback to the MSF method is that it is more expensive and is less time efficient than the SSF method since the formed part is replaced on every iteration.

In order to form a part accurately it is crucial to maximize controllability of the reference geometry. Features such as unsupported angles can cause inaccuracies that dominate the geometric error of the part and must be eliminated to achieve acceptable results. Reductions in error of up to 72.7% were observed by offsetting the reference in order to increase its controllability. As such, reference geometries must be examined carefully in order to ensure their resultant controllability will allow for effective use of the selected control algorithm.

Finally, it was shown that larger correction factors led to a faster convergence at the cost of a lower part accuracy. The reduction in accuracy is a result of the control algorithm having a reduced number of iterations in which to correct the part before over forming occurs. As a result, its ability to correct the part is reduced when the iterations decrease from an increased correction factor. It is important that the correction factor is selected for the appropriate application.

References

[1] A. K. Behera, R. A. D. Sousa, G. Ingarao, and V. Oleksik, "Single point incremental forming: An assessment of the progress and technology trends from 2005 to 2015," *Journal of Manufacturing Processes*, vol. 27, pp. 37–62, 2017.

[2] E. Hagan and J. Jeswiet, "A review of conventional and modern single-point sheet metal forming methods," *Proceedings of the Institution of Mechanical Engineers, Part B: Journal of Engineering Manufacture*, vol. 217, no. 2, pp. 213–225, 2003.

[3] J. Jeswiet, "Asymmetric Incremental Sheet Forming," *Sheet Metal 2005 Advanced Materials Research*, pp. 35–58, 2005.

[4] H. Lu, "Investigation of Control of the Incremental Forming Processes," thesis, School of Mechanical and Mining Engineering, 2017.

[5] F. Micari, G. Ambrogio, and L. Filice, "Shape and dimensional accuracy in Single Point Incremental Forming: State of the art and future trends," *Journal of Materials Processing Technology*, vol. 191, no. 1-3, pp. 390–395, 2007.

[6] A. Fiorentino, G. Feriti, E. Ceretti, C. Giardini, C. Bort, and P. Bosetti, "Development of Tool Path Correction Algorithm in Incremental Sheet Forming," *Key Engineering Materials*, vol. 622-623, pp. 382–389, Sep. 2014.

[7] A. Fiorentino, E. Ceretti, G. C. Feriti, and C. Giardini, "Improving Accuracy in Aluminum Incremental Sheet Forming of Complex Geometries Using Iterative Learning Control," *Key Engineering Materials*, vol. 651-653, pp. 1096–1102, Oct. 2015.

[8] K. Suresh, A. Khan, and S. P. Regalla, "Tool Path Definition for Numerical Simulation of Single Point Incremental Forming," *Procedia Engineering*, vol. 64, pp. 536–545, Mar. 2013.

[9] N. Decultot, L. Robert, V. Velay, and G. Bernhart, "Single point incremental sheet forming investigated by in-process 3D digital image correlation," *EPJ Web of Conferences*, vol. 6, p. 11001, Jun. 2010.

[10] P. Eyckens, B. Belkassem, C. Henrard, J. Gu, H. Sol, A. M. Habraken, J. R. Duflou, A. V. Bael, and P. V. Houtte, "Strain evolution in the single point incremental forming process: digital image correlation measurement and finite element prediction," *International Journal of Material Forming*, vol. 4, no. 1, pp. 55–71, 2010.

[11] S. Arimoto, S. Kawamura, and F. Miyazaki, "Bettering operation of Robots by learning," *Journal of Robotic Systems*, vol. 1, no. 2, pp. 123–140, Mar. 1984.

[12] M. Callegari, A. Gabrielli, M.-C. Palpacelli, and M. Principi, "Incremental Forming of Sheet Metal by Means of Parallel Kinematics Machines," *Journal of Manufacturing Science and Engineering*, vol. 130, no. 5, p. 054501, Aug. 2008.

[13] H. Lu, M. Kearney, Y. Li, S. Liu, W. J. T. Daniel, and P. A. Meehan, "Model predictive control of incremental sheet forming for geometric accuracy improvement," *The International Journal of Advanced Manufacturing Technology*, vol. 82, no. 9-12, pp. 1781–1794, Nov. 2015.

[14] B. Friedland, *Control system design: an introduction to state-space methods*. Mineola: Dover Publications, Inc., 2005.

[15] W. Emmens, G. Sebastiani, and A. V. D. Boogaard, "The technology of Incremental Sheet Forming—A brief review of the history," *Journal of Materials Processing Technology*, vol. 210, no. 8, pp. 981–997, Feb. 2010.

[16] K. Jackson and J. Allwood, "The mechanics of incremental sheet forming," *Journal of Materials Processing Technology*, vol. 209, no. 3, pp. 1158–1174, Mar. 2009.

[17] Norrlöf Mikael, "Iterative learning control: analysis, design, and experiments," dissertation, 2000.